Hindawi
Advances in Civil Engineering
Volume 2023, Article ID 7320049, 9 pages
https://doi.org/10.1155/2023/7320049

Research Article

Rainfall Scouring Mechanism of the High-Speed Railway Subgrade Slope with Coarse-Grained Soil

Shao-Wei Wei,[1,2] De-Gou Cai,[1] Song Lv ,[1,2] Jian-Jie Jiang,[3] and Zhen-Dong Cui [3]

[1]*Railway Engineering Research Institute, China Academy of Railway Sciences Corporation Limited, Beijing 100081, China*
[2]*Beijing Tieke Special Engineering Technology Corporation Limited, Beijing 100081, China*
[3]*State Key Laboratory for Geomechanics and Deep Underground Engineering, School of Mechanics and Civil Engineering, China University of Mining and Technology, Xuzhou 221116, Jiangsu, China*

Correspondence should be addressed to Song Lv; lvsongok@126.com

Received 30 May 2023; Revised 17 October 2023; Accepted 18 October 2023; Published 9 November 2023

Academic Editor: Xing Wang

The hydraulic erosion of the subgrade slope can lead to serious loss of filling materials and landslides, affecting stability. In particular, there is no quantitative consideration of the scouring calculation method for the design codes of High-Speed Railway Subgrade Slope (HRSS). This paper mainly focuses on the anti-erosion stability of HRSS with coarse-grained soil and analyzes the current research shortcomings. The scouring on the subgrade slope was analyzed by establishing an incipient flow velocity formula that optimized the derivation process and parameters. Compared with the two types of cases, the exactitude of the formula derivation is verified. Finally, combined with orthogonal grouping, a single-factor analysis was conducted on the slope gradient and soil shear strength. With the same particle size, the incipient flow velocity decreases with the increase of the slope gradient (29.7° – 45°). When the particle size is upwards of 0.1 mm, the slope gradient has a great impact on the incipient flow velocity. And as the slope gradient decreases, the acceleration of incipient flow velocity with the same particle size increases. The incipient flow velocity increases with the increase of C (Cohesion) or φ (internal friction angle). The value of φ influences more deeply in the particle size range of 0.1 – 20 mm, that is, to advance the resisting erosion capacity, the shear strength of the slope soil is encouraged to improve when designing slope protection measures.

1. Introduction

High-Speed Railway Subgrade Slope (HRSS), shown in Figure 1, perennially exposed to the natural environment, is prone to instability under rainfall. Landslides caused by the rainfall infiltration or erosion failure are the main issues that lead to slope instability and other foundation risks [1–5]. Some measures are adopted to reduce the possibility of landslides and erosion problems, including ecological protection and masonry protection. The slope instability caused by rainfall infiltration has been studied comprehensively [6]. HRSS is divided into embankment slopes and cutting slopes. The height and slope gradient directly determine the rainfall area, affecting the incipient flow velocity induced by erosion on the slope surface. Referring to the "Code for Design of High-Speed Railways" (TB10621-2014) [7], the height of embankment slopes for high-speed railways generally does not exceed 20 m, the upper height does not exceed 12 m, and the slope ratio is 1 : 1.5. The lower part shall not exceed 8 m in height, with a slope rate of 1 : 1.75, and the slope form shall be a broken line or stepped type. Depending on the engineering performance and grading characteristics, subgrade slope fillers can be divided into groups A, B, C, and D. Fillers of HRSS mainly use groups A and B fillers, coarse-grained soil. Nevertheless, there is room for improvement in the calculating system of erosion failure for subgrade slopes in the design codes. Rainfall erosion often happens on the slope surface, such as sheet erosion and rills. As the continuous and multiple scouring, erosion will further develop into the interior of the subgrade, resulting in landslides [8–10]. Therefore, the erosion failure of the subgrade slope which may lead to serious security risks should be quantitatively studied.

Closely related to the disciplines such as soil science, soil mechanics, hydraulics, and sediment dynamics, erosion issues

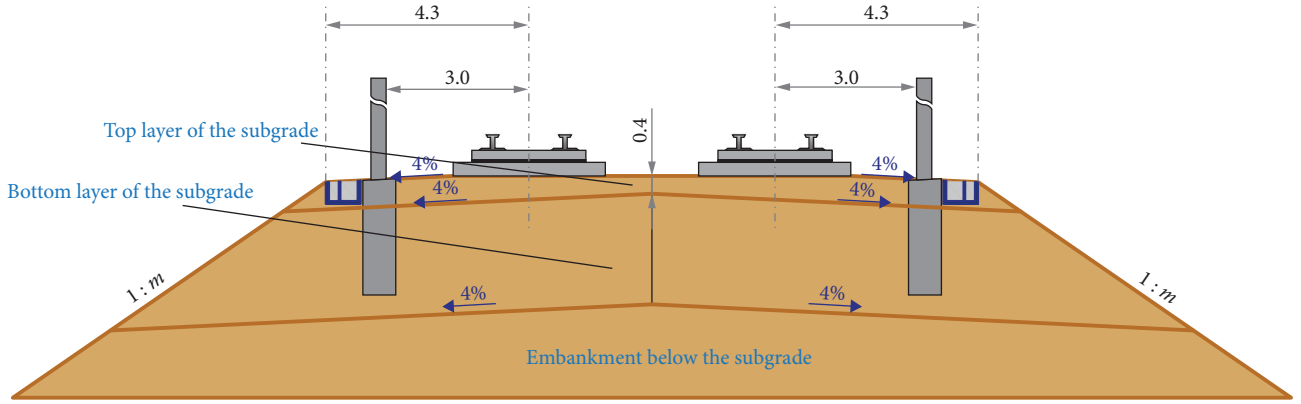

Figure 1: The structure design of HRSS in TB10621-2014.

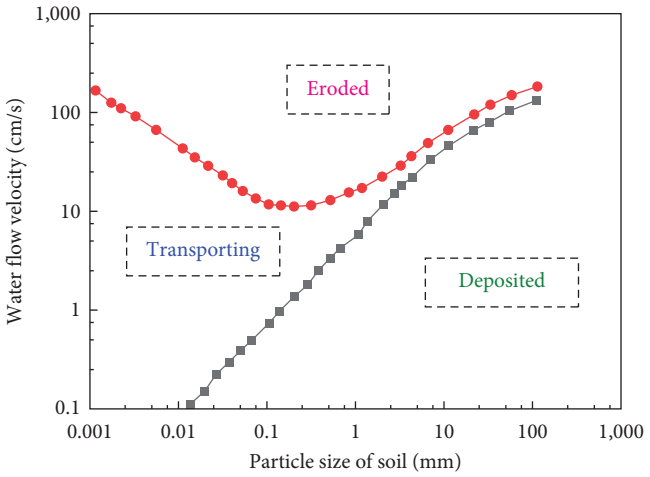

Figure 2: Critical states of erosion depend on the flow velocity and the particle size [12].

are affected by various factors [11, 12]. Soil particles may be scoured out of the slope surface under the direct impact of rainwater and the drag force of the water flow, which should be quantitatively analyzed based on the particle size and the flow velocity. According to the German research results, Figure 2 noted the critical states of erosion for soil particles, which depend on the functional relationship between the soil particle size and flow velocity [13, 14]. Since the second half of the 19th century, people have deeply realized the necessity of quantitative research on soil erosion, and are eager to try to establish a simple and efficient mathematical method for quantitative prediction [15–17]. Based on the observations in 10,000 areas over 30 years, the Universal Soil Loss Equation (USEL) [18, 19] was extensively used in predicting the average annual soil erosion in the United States. The design codes in Japan and China only mention some subgrade slope protection measures but do not mention the anti-erosion stability analysis method of subgrade slope caused by rainfall. The slope protection engineering of HRSS includes ecological protection and engineering protection. The engineering protection measures mainly include physical slope protection (wall), skeleton slope protection, anchor rod (cable) frame beam slope protection, and sprayed concrete slope protection. The ecological protection measures mainly include various forms such as spraying grass, planting belt (bag) grass, and guest soil planting.

The recent research on subgrade slope erosion mainly focuses on the mechanism of erosion starting, the erosion process and calculating the scouring amount. Based on the conversion relationship between the flow velocity field and shear field and the feature of erosion for granite eluvium cutting slope, a calculating formula model, including the drag force and the flow velocity, was established by Luo et al. [20]. However, the cohesion force, one of the parameters for soil, was not considered. Depending on the soil characteristics, the homogeneity and cohesion of soil on slopes were classified and discussed by Wang [21] to analyze the critical conditions for subgrade slopes notionally. Based on the law of energy conservation, a slope erosion calculation model was put forward by Li et al. [22], who compared the quantity of soil loss calculated by his model with the data of the erosion amount obtained by the on-site measure, which verified that the model had a good prediction effect. Figuring out the influencing factors of rainfall erosion and the hydraulic erosion process, an erosion calculation model and the evaluation method for railway slope proposed by Kuang [23] to optimize slope protection measures. To promote the calculating model, Guo [24] analyzed the mechanism of slope erosion initiation of cohesionless filler and cohesive filler, taking into account the structure of railway subgrade, filler, rainfall, and catchment characteristics, and obtained the variation rules of slope velocity and threshold particle size with rainfall intensity. Model tests are commonly used to study slope instability, due to the frequent use of artificial rainfall erosion in the experiments, which is often limited to the implementation of local rainfall patterns, there is a boundary constraint effect between the rainfall area and the non-rainfall area, manifested as the lateral infiltration of rainwater and the lag of slope deformation in the non-rainfall area on the rainfall area. A deep-buried isolation trench test method has been proposed to address these boundary effects [25]. The problem with the existing rainfall warning system for the prevention of railway disasters is that the determination of rainfall warning values is mainly by statistical data or experience, so lacking deep analysis of

the mechanism of slope topsoil disaster induced by rainfall [26]. This situation causes the rainfall warning values to not match actual disaster grades. The main railway subgrade slope disaster is topsoil slip during rainy days.

To sum up, the existing scouring starter theory has not comprehensively pondered the soil properties, and the scouring starter formula does not fully reflect the soil-related parameters. Furthermore, existing formulas for the initiation of slope erosion are often derived indirectly through certain assumptions using the conversion from the horizontal surface to the slope surface, resulting in miscalculation. The coarse-grained soil, with firm water permeability and high-compressive strength, is normally applied to high-speed railway subgrade engineering. This paper quantitatively deduced and verified a formula for critical incipient flow velocity of scouring of HRSS with coarse-grained soil induced by rainfall erosion. On this basis, the erosion mechanism for soil particles has been clarified.

2. Basic Assumptions

To optimize the derivation process, the basic assumptions are as follows:

(1) The soil particles are spherical;
(2) When the water flow satisfies the Bernoulli principle, and the soil particles leave the slope height relative to three times the particle size, the uplifting force basically disappears;
(3) The intergranular action, charge gravity, bite force, cementation force, and cohesion of soil particles and shear strength parameters are uniformly simplified to adhesion;
(4) The surface infiltration conditions of the slope surface are good, and the infiltration pressure is consistent with the infiltration direction;
(5) The direction of rainfall is the same as the direction of gravity;
(6) When the critical start of scouring, the friction resistance flow rate is a fixed value;
(7) When the critical start of scouring, the friction coefficient is a constant fixed value;
(8) The critical starting of scouring is static;
(9) The slope erosion is a strong turbulent effect, and the viscosity of the water flow is not considered;
(10) The length of turbulence mixing can be determined using Carmen's turbulence similarity hypothesis.

3. Derivation of the Critical State of Velocity Scouring Formula on the Slope Surface

3.1. Force Analysis for Soil Particles on the Slope. Under the action of water flow, soil particles on the slope surface of the subgrade are subjected to the floating gravity w' (N), the drag force F_D (N), the lift force F_L (N), and the infiltration pressure F_S (N) and cohesion C (N).

$$w' = (\gamma_s - \gamma_w)\frac{\pi D^3}{6}, \tag{1}$$

where γ_s is the unit weight of soil particles (N/m^3); γ_w is the unit weight of water (N/m^3); D is the grain size (m).

On the basis of sediment motion mechanics, drag forces and lift forces are exerted by liquid phase water flow on solid particles. During the water scouring, friction will occur when the water scours the surface of soil particles. When the Reynolds number of the water flows is slightly higher, the streamlines at the top of the soil particles will separate, and vortices will exist on the surface of the soil particles, resulting in a pressure differential between the front and rear of the soil particles, forming the form resistance. The drag force F_L is the combination of the friction induced by water flow on the surface of soil particles and the shape resistance generated by vortices. In light of Bernoulli's principle, when water flows on the slope, the velocity at the top of the soil particles is significantly greater than the velocity of the infiltration flow between the soil particles at the bottom, resulting in an uplift force F_L.

$$F_D = C_D\frac{\pi D^2}{4}\frac{\rho u_0^2}{2}, \tag{2}$$

$$F_L = C_L\frac{\pi D^2}{4}\frac{\rho u_0^2}{2}, \tag{3}$$

where C_D is the drag force coefficient; C_L is the lift force coefficient; ρ is the density of water (kg/m^3); u_0 is the velocity of flow on the soil surface (m/s).

After the soil particles leave the slope and move in a push mode, on the one hand, they begin to be subjected to upper water with faster flow velocity, resulting in increasing the drag force, and on the other hand, the lift force tends to disappear due to a decrease in the pressure differential between the upper and bottom sides of the particles.

When rainfall accumulates on the slope, the infiltration pressure F_S generated by the infiltration of the slope surface is consistent with the infiltration direction.

$$F_S = \gamma_w J_S\frac{\pi D^3}{6}, \tag{4}$$

where J_s is the hydraulic gradient of infiltration flow in soil. For unsaturated soil slopes, when the slope gradient is relatively gentle, the seepage pressure enhances the stability of soil particles. Nevertheless, when the slope gradient is steep, the component of seepage pressure along the flow direction will intensify slope erosion.

According to the soil mechanics theory, the positive charge of the water molecule, attracted by the surface of soil particles with negative charges, is aligned to form binding water, generating cohesion C. Besides, C may exist from the cementation of soil particles by substances such as silicon, iron, and carbonate contained in the soil.

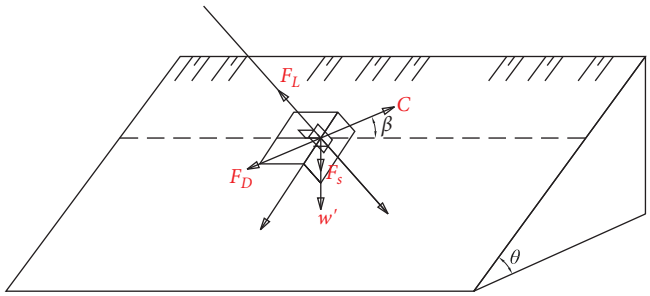

FIGURE 3: The force analysis for soil particles on the surface of the slope.

3.2. The Critical State for the Starting. Figure 3 demonstrates the force analysis for the soil particles on the slope. The combined force of infiltration pressure F_S and the floating gravity w' is, among the slope direction and perpendicular to the slope direction, $(F_S + w')\sin\theta$ and $(F_S + w')\cos\theta$ separately. Compared with the force mode under horizontal plane conditions, the floating weight, with the component force in the slope direction, exacerbates the erosion of the slope. Besides, contrary to the direction of F_D, the angle between C and the slope axis is β.

The F_D for soil particles in the direction $\beta = 90°$ can be determined as follows:

$$F_D = \tan\varphi[(w' + F_S)\cos\theta - F_L] - (w' + F_S)\sin\theta + C, \tag{5}$$

where φ is the interior friction angle.

Substituting Equations (1)–(4) into Equation (5) yields:

$$\rho u_0^2(C_D + \tan\varphi CL) = \frac{4D}{3}[(\gamma_s - \gamma_w + \gamma_w J_s)(\tan\varphi\cos\theta - \sin\theta) + 6C/(\pi D^3)], \tag{6}$$

where $u_0 = U_R \cdot f_i(U_R \cdot D/\nu)$; U_R is the frictional velocity; and $U_R = (\tau_c/\rho)^{0.5}$; $f_i(U_R \cdot D/\nu)$ is the function of Reynolds number. The critical state of drag force can be obtained as follows:

$$\tau_c = \frac{4D[(\gamma_s - \gamma_w + \gamma_w J_s)(\tan\varphi\cos\theta - \sin\theta) + 6C/(\pi D^3)]}{3(C_D + \tan\varphi\, CL)[f_i(U_R \cdot D/\nu)]^2}, \tag{7}$$

where

$$f\left(\frac{U_R \cdot D}{\nu}\right) = \frac{4}{3(C_D + \tan\varphi\, CL)[f_i(U_R \cdot D/\nu)]^2}. \tag{8}$$

Substituting Equation (8) into Equation (7) yields:

$$\tau_c = f(U_R \cdot D/\nu)[(\gamma_s - \gamma_w + \gamma_w J_s)(\tan\varphi\cos\theta - \sin\theta) + 6C/(\pi D^3)]D. \tag{9}$$

From Equation (9), the critical state of drag force for soil particles is primarily determined by the soil particle size, the slope gradient, the internal friction angle, and cohesion.

For the laminar flow, the relationship between the flow velocity and the flow shear force can be simply determined as follows:

$$\tau = \mu\frac{du}{dy} = \nu\rho\frac{du}{dy}, \tag{10}$$

where μ is the coefficient of viscosity for water; u is the flow velocity (m/s); τ is the flow shear force (Pa); y is the distance from the flow section to the slope surface (m); and ν is the dynamic viscosity coefficient.

For the turbulent flow, the shear force of the flow is much more complex. Based on the mixing length theory for turbulent flow, the fluctuating velocity among the flowing direction and depth direction can be obtained, respectively:

$$u' = l\frac{du}{dy}_{y=y}, \tag{11}$$

$$v' = l\frac{du}{dx}, \tag{12}$$

where l is the mixing length of turbulent flow (m).

Based on the fluid mechanics, the turbulent shear formula can be determined as follows:

$$\tau = -\rho u'v'. \tag{13}$$

Substituting Equations (11) and (12) into Equation (13) yields:

$$\tau = \rho l^2\left(\frac{du}{dy}\right)^2. \tag{14}$$

When the turbulence of water flow is weak, the water flow shear force should be the sum of the viscous shear force and the turbulent shear force as follows:

$$\tau = \mu\frac{du}{dy} + \rho l^2\left(\frac{du}{dy}\right)^2. \tag{15}$$

However, it is unnecessary to consider the viscous force of water flow in the analysis of slope erosion owing to its strong turbulence.

The turbulent mixing length can be determined by Kármán's turbulent similarity hypothesis. Assuming that the flow velocities at the distances of y_1 and y_2 from the slope surface are u_1 and u_2, respectively, the variation of which can be determined as follows:

$$lu(y_1 + \mathrm{d}y) = u_1 + \frac{\mathrm{d}u_1}{\mathrm{d}y}\mathrm{d}y + \frac{1}{2}\frac{\mathrm{d}^2u_1}{\mathrm{d}y^2}\mathrm{d}y^2 + \frac{1}{6}\frac{\mathrm{d}^3u_1}{\mathrm{d}y^3}\mathrm{d}y^3 + \ldots u(y_2 + \mathrm{d}y) = u_2 + \frac{\mathrm{d}u_2}{\mathrm{d}y}dy + \frac{1}{2}\frac{\mathrm{d}^2u_2}{\mathrm{d}y^2}dy^2 + \frac{1}{6}\frac{\mathrm{d}^3u_2}{\mathrm{d}y^3}\mathrm{d}y^3 + \ldots. \tag{16}$$

According to Kármán's turbulent similarity hypothesis, there is the following relationship:

$$\frac{\mathrm{d}u_2/\mathrm{d}y}{\mathrm{d}u_1/\mathrm{d}y} \propto \frac{\mathrm{d}^2u_2/\mathrm{d}y^2}{\mathrm{d}^2u_1/\mathrm{d}y^2} \propto \frac{\mathrm{d}^3u_2/\mathrm{d}y^3}{\mathrm{d}^3u_1/\mathrm{d}y^3} \propto \ldots, \tag{17}$$

and

$$\frac{\mathrm{d}u/\mathrm{d}y}{\mathrm{d}^2u/\mathrm{d}y^2} = \frac{l}{k}. \tag{18}$$

The turbulent mixing length can be obtained as follows:

$$l = k\frac{\mathrm{d}u/\mathrm{d}y}{\mathrm{d}^2u/\mathrm{d}y^2}, \tag{19}$$

where k is the proportional coefficient, that is, the Kármán constant.

The velocity field can be obtained as follows:

$$\tau = \rho k^2 \frac{(\mathrm{d}u/\mathrm{d}y)^4}{(\mathrm{d}^2u/\mathrm{d}y^2)^2}. \tag{20}$$

The linear distribution of shear force along a vertical line in a two-dimensional flow can be determined as follows:

$$\tau_y = \tau_0\left(1 - \frac{y}{h}\right), \tag{21}$$

where τ_y is the water flow shear force at the distance of y from the slope surface (Pa); τ_0 is the water flow shear force at the slope surface (Pa).

Substituting Equation (20) into Equation (21) yields:

$$\frac{u_h - u_y}{U_R} = -\frac{1}{k}\left\{\left(1 - \frac{y}{h}\right)^{1/2} + \ln\left[1 - \left(1 - \frac{y}{h}\right)^{1/3}\right]\right\}, \tag{22}$$

where u_h is the flow velocity at the water flow surface (m/s); u_y is the flow velocity at the distance of y from the slope surface (m/s).

When U_R remains constant, $(u_h - u_y)$ can be considered only varied with y. Besides, near the slope surface where erosion occurs, the flow shear force, varied insignificantly, can be approximated as equal to the slope shear force τ_0.

$$\frac{\mathrm{d}^2u/\mathrm{d}y^2}{(\mathrm{d}u/\mathrm{d}y)^2} = -k/U_R. \tag{23}$$

The vertical velocity distribution formula for slope flow can be obtained as follows:

$$\frac{u_y}{U_R} = \frac{1}{k}\ln\left(\frac{y}{y_0}\right), \tag{24}$$

where y_0 is the distance from the slope surface where the velocity of water flow is equal to zero (m).

Integrating Equation (24), the average velocity of the water flow section, divided into two situations, can be obtained:

(1) Smooth slope surface

$$\frac{U}{U_R} = 3.25 + 5.75\log\left(\frac{R \cdot U_R}{\nu}\right), \tag{25}$$

(2) Rough slope surface

$$\frac{U}{U_R} = 6.25 + 5.75\log\left(\frac{R}{k_s}\right), \tag{26}$$

where U is the average velocity of the water flow section (m/s); R is the hydraulic radius (m); k_s is the surface roughness (m).

Considering the roughness of the slope surface, Equation (26) is transformed as follows:

$$U = 5.75U_R \cdot \log\left(12.27\frac{\chi R}{k_s}\right) = 5.75\sqrt{\frac{\tau_c}{\rho}}\log\left(12.27\frac{\chi R}{k_s}\right), \tag{27}$$

where χ is the correction coefficient.

Substituting Equation (9) into Equation (27) yields:

$$U = 5.75\sqrt{\frac{\left[(\gamma_s - \gamma_w + \gamma_w J_s)(\tan\varphi\cos\theta - \sin\theta) + \frac{6C}{\pi D^3}\right] f\left(\frac{U_R D}{\nu}\right) gD}{\gamma_w}}\log\left(12.27\frac{\chi R}{k_s}\right). \tag{28}$$

4. Case Study and Equation Verification

To verify the accuracy of Equation (28), a comparison is conducted with some case studies, including horizontal channel cases and a subgrade case.

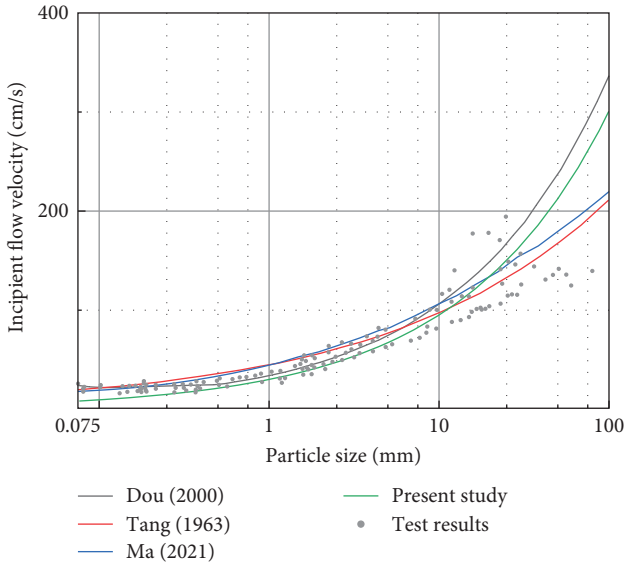

Figure 4: Comparison between others' equations, test results and the present study.

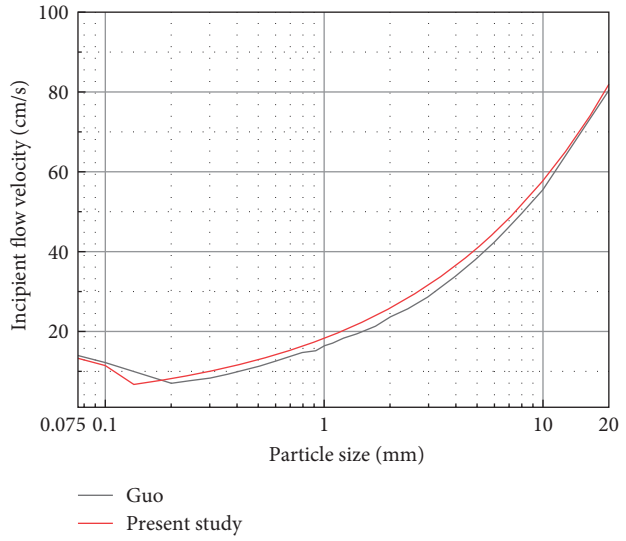

Figure 5: Comparison between Guo's equation and the present study for the subgrade slope.

4.1. Verification by Field Tests and Equations of the Horizontal Slope ($\theta = 0°$). The same parameters and filed data, conducted by Dou [27], are used for the comparison. Moreover, some empirical formulas for incipient flow velocity on the horizontal slope were proposed by Dou [27] and Ma [28], respectively. The unit weight of soil particles γ_s is 26.5 kN/m^3. The interior friction angles φ and cohesion C equal 38° and 0 kN, respectively. The correction coefficient χ is taken for 1, and the hydraulic radius R is 0.15 m. The surface roughness k_s and the function of Reynolds number $f(U_R{\cdot}D/\nu)$ equal 0.005 and 0.04, respectively. For the coarse-grained soil, size between 0.075 and 20 mm, the curve of the present study is located at the lower edge of the test results or other empirical formulas, shown in Figure 4, which is in good agreement with the test results.

4.2. Verification by the Equation of the Subgrade Slope ($\theta = 33.7°$). The formula in this paper is directly derived from the soil particles on the subgrade slope, instead of assuming the transformation relationship from the horizontal surface to the slope surface. The same parameters in the calculation formula for the subgrade slope, conducted by Guo [24], are used for comparison, shown in Figure 5. The unit weight of soil particles γ_s is 26.5 kN/m^3. The interior friction angles φ and cohesion C equal 38° and 20 kN, respectively. The correction coefficient χ is taken for 1, and the hydraulic radius R is 0.015 m. The surface roughness k_s and the function of Reynolds number $f(U_R{\cdot}D/\nu)$ equal 0.005 and 0.04, respectively. For the whole size between 0.075 and 20 mm, the curve of the present study is in good agreement with Guo's empirical equation. In the vast majority of the curve, the maximum difference between Guo's and the present study is within 5%.

To sum up, the incipient flow velocity equation for soil particles in this paper is not only suited for the horizontal slope but also has a high accuracy for the subgrade slope.

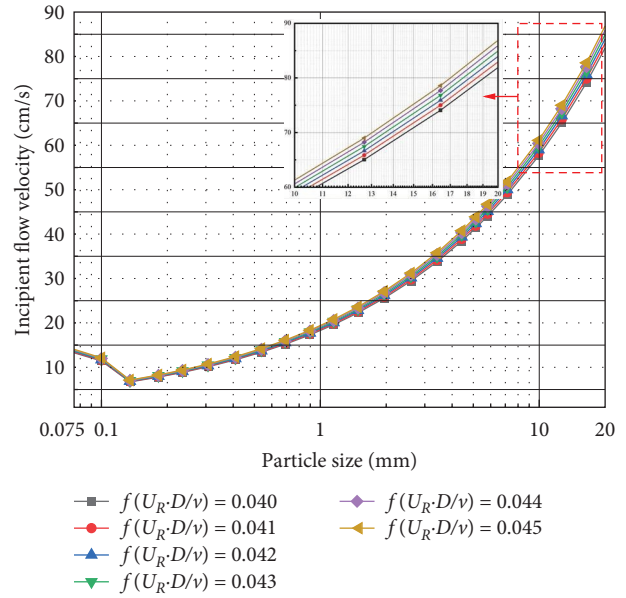

Figure 6: The incipient flow velocity under different Reynolds number.

5. Analysis of Impact Factors of the Incipient Flow Velocity

5.1. The Incipient Flow Velocity under Different Reynolds Number. The incipient flow velocity varies with different Reynolds numbers, shown in Figure 6. The unit weight of soil particles γ_s equals 26.5 kN/m^3. The interior friction angles φ and cohesion C equal 38° and 20 kN, respectively. The correction coefficient χ is taken for 1, and the hydraulic radius R is 0.015 m. The surface roughness k_s and the slope gradient θ equal 0.005° and 33.7°, respectively.

For coarse-grained soil, the function of Reynolds numbers is usually taken as 0.04–0.045. Thus, in this range, with

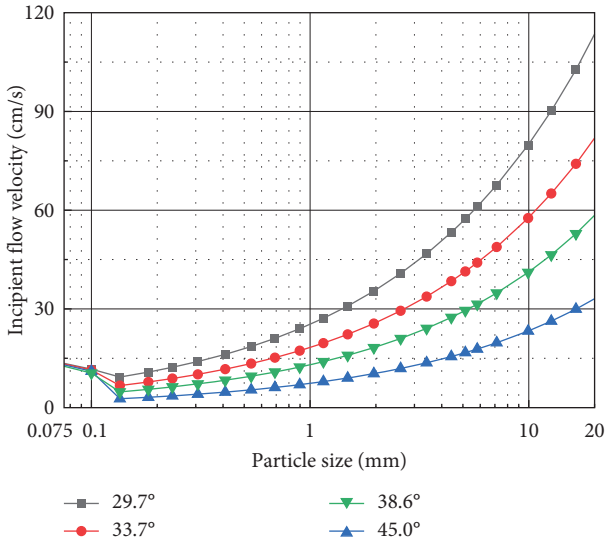

Figure 7: The incipient flow velocity under different slope gradients.

the same particle size, the incipient flow velocity increases with the increase of the $f(U_R{\cdot}D/v)$ but impacts less. Thus, the $f(U_R{\cdot}D/v)$ is taken as 0.04 in the following analysis.

5.2. The Incipient Flow Velocity under Different Slope Gradients. To analyze the affection of slope gradients to the incipient flow velocity, four common subgrade slope gradients ($\tan\theta$) are shown in Figure 7. The incipient flow velocity under different slope gradients is shown in Figure 7. The unit weight of soil particles γ_s equals 26.5 kN/m^3. The interior friction angles φ and cohesion C equal 38° and 20 kN, respectively. The correction coefficient χ is taken for 1, and the hydraulic radius R is 0.015 m. The surface roughness k_s and the function of Reynolds number $f(U_R{\cdot}D/v)$ equal to 0.005 and 0.04, respectively.

With the same particle size, the incipient flow velocity decreases with the increase of the slope gradient. When the particle size is less than 0.1 mm, the incipient flow velocity is slightly affected by the slope gradient, conversely, the slope gradient has a great impact on it. And as the slope gradient decreases, the acceleration of the incipient flow velocity with the same particle size increases.

5.3. The Incipient Flow Velocity under Different C or φ. The orthogonal grouping of C and φ was conducted to analyze the affection of soil shear strength on the incipient flow velocity on the slope, shown in Table 1 and Figure 8. The unit weight of soil particles γ_s and the slope gradient θ equal 26.5 kN/m^3 and 33.7°, respectively. The correction coefficient χ is taken for 1, and the hydraulic radius R is 0.015 m. The surface roughness k_s and the function of Reynolds number $f(U_R{\cdot}D/v)$ equal 0.005 and 0.04, respectively.

The incipient flow velocity increases with the increase of C or φ. The value of C impacts greater in the particle size range of 0.075–0.1 mm, while the value of φ influences more deeply in the particle size range of 0.1–20 mm. With the φ decreasing by 20.8%, the incipient flow velocity of Group 3 is much larger than that of Group 5 or Group 8, although the C increases to 200%.

Table 1: The orthogonal grouping of C and φ.

Group number	C (kN)	φ (°)
1	10	28
2	10	38
3	10	48
4	20	28
5	20	38
6	20	48
7	40	28
8	40	38
9	40	48

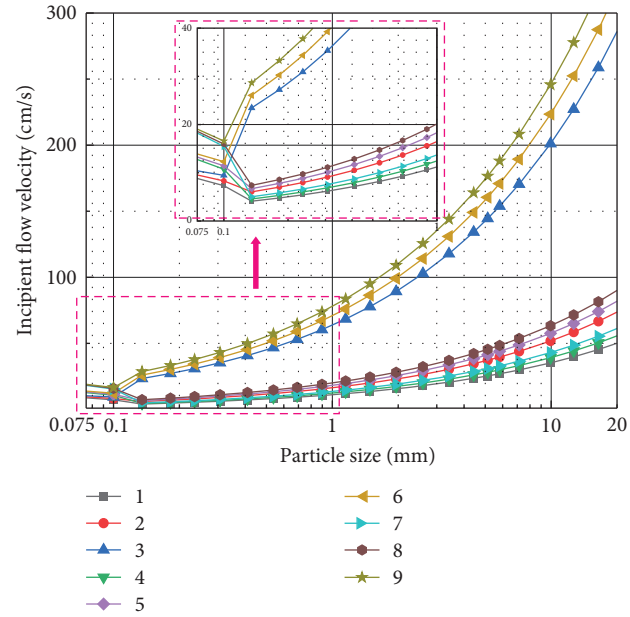

Figure 8: The incipient flow velocity under different C or φ.

5.4. The Incipient Flow Velocity under Different Slope Height. Considering the impact of slope height, the issue has been simplified by comparing the incipient flow velocity for the same soil size on different parts of the slope surface. In this paper, the derivation of the incipient flow velocity is based on soil particles at any position on the slope as the research object. Therefore, the incipient flow velocity for soil particles with the same particle size will not change with the change in slope height. Nevertheless, under the same rainfall intensity, affected by gravity, rainwater flow speed accelerates along the slope. The higher the slope height, the faster the flow velocity at the toe of the slope is, resulting in more severe erosion. Thus, in further research, establishing the relationship between the incipient flow velocity and rainfall intensity, the influence of slope height can be quantitatively calculated.

6. Discussion

In this paper, the incipient flow velocity of HRSS with coarse-grained soil is studied induced by rainfall erosion, based on theoretical derivation and numerical analysis. In

terms of applicability, the formula applies to situations where cohesive soil is present on slope surfaces or horizontal river channels. The masonry skeleton, often used on the subgrade slope, is a common method to reduce the rainfall erosion. Thus, with the incipient flow velocity equation established in this paper, we can quantitatively calculate the erosion condition. The spacing of masonry skeleton can be optimized by combining past measured results to reduce costs. The value of C and φ mainly comes from practical engineering experience. An indoor rainfall erosion model test, which operates the essential process, will be conducted and summarized to optimize parameters and validate the formula. In addition, under the same slope height, a change in slope gradient will inevitably change the rainfall area on the slope surface. Although the incipient flow velocity of filler particles decreases with the increase of slope gradient, at the same time, the rainfall area reduces on the slope, which leads to the decrease of the slope runoff. Thus, the impact of slope gradient on the stability of slope erosion resistance needs further research. The flow velocity and raindrop impact are closely related to the rainfall intensity. The raindrop impact and the sheet flow resistance caused by raindrop impact also influence the starting of soil particles [29, 30]. By establishing the quantitative relationship between the flow velocity, raindrop impact and rainfall intensity, the impact of rainfall intensity on the incipient particle size can be figured out. The surface soil on the slope is composed of soil particles with different particle sizes. When analyzing the slope instability under erosion, it is necessary to consider determining the grading criteria or combining random theory for research. Many factors affect the stability of HRSS, such as rainfall characteristics, slope morphology characteristics, slope rock and soil properties, and slope protection measures. The stability evaluation of slope erosion is complex, involving significant uncertainty. Recently, many research methods concentrate on using fuzzy mathematics and neural networks to conduct stability analysis. Subsequently, after finishing model tests, our team will establish the database for HRSS instability induced by erosion with the evaluation indicators, including quantitative, semiquantitative, and qualitative evaluation methods.

7. Conclusion

There are few studies on the incipient flow velocity of HRSS. An optimized formula, considering the cohesion of coarse-grained soil, is established by deriving directly on the subgrade slope. The incipient flow velocity equation for soil particles in this paper is not only suited for the horizontal slope but also has a high accuracy for the subgrade slope. The main conclusions are as follows:

(1) This article studies the erosion initiation law of HRSS and establishes the incipient flow velocity equation suitable for multiple working conditions, including coarse-grained soil subgrade slopes with different slope gradients.

(2) Different flow velocities induced by rainfall result in different spacing of masonry skeleton on the subgrade slope. The equation incipient flow velocity can be adopted to optimize the spacing of the masonry skeleton to reduce costs.

(3) Compared with the existing empirical formulas for subgrade slope, the accuracy in the present study has been verified.

(4) With the same particle size, the incipient flow velocity decreases with the increase of the slope gradient. When the particle size is less than 0.1 mm, the incipient flow velocity is slightly affected by the slope gradient, conversely, the slope gradient has a great impact on it. And as the slope gradient decreases, the acceleration of incipient flow velocity with the same particle size increases.

(5) The incipient flow velocity increases with the increase of C or φ. The value of C impacts greater in the particle size range of 0.075–0.1 mm, while the value of φ influences more deeply in the particle size range of 0.1–20 mm. With the φ decreasing by 20.8%, the incipient flow velocity of Group 3 ($C = 10$ kN, $\varphi = 48$) is much larger than that of Group 5 ($C = 20$ kN, $\varphi = 38°$) or group 8 ($C = 40$ kN, $\varphi = 38°$), although the C increases to 400%.

(6) The research results on the starting flow rate in this article can provide a theoretical basis for the protection of HRSS. The shear strength of the slope soil is encouraged to improve when designing slope protection measures.

Data Availability

The data that support the findings of this study are available from the corresponding author upon reasonable request.

Conflicts of Interest

The authors declare no conflicts of interest.

Acknowledgments

This work was supported by the Scientific Research Project of China Academy of Railway Sciences Co., LTD (2021YJ070).

References

[1] J. Han, J. Wang, D. Jia et al., "Construction technologies and mechanical effects of the pipe-jacking crossing anchor-cable group in soft stratum," *Frontiers in Earth Science*, pp. 1–19, 2023.

[2] J. Wang, J. Han, J. Chen et al., "Experimental and numerical study on the dynamic response of a superthick backfill subgrade under high-speed railway loading: a case study of Qianjiang—Zhangjiajie—Changde Railway," *Journal of Construction Engineering and Management*, vol. 148, no. 12, Article ID 5022014, 2022.

[3] G. J. Guo, G. H. Liu, J. Sui, and J. Q. Wu, "Subgrade slope stability analysis under the condition of rainfall infiltration," *Applied Mechanics and Materials*, vol. 353-356, pp. 1073–1076, 2013.

[4] Z. Liu, "Influence of rainfall characteristics on the infiltration moisture field of highway subgrades," *Road Materials and Pavement Design*, vol. 16, no. 3, pp. 635–652, 2015.
[5] Z. Guo and Z. Zhao, "Numerical analysis of an expansive subgrade slope subjected to rainfall infiltration," *Bulletin of Engineering Geology and the Environment*, vol. 80, no. 7, pp. 5481–5491, 2021.
[6] J.-J. Jiang and Z.-D. Cui, "Instability of high liquid limit soil slope for the expressway induced by rainfall," *Applied Sciences*, vol. 12, no. 21, Article ID 10857, 2022.
[7] Ministry of Railways of the People's Republic of China, *Code for Design of High-Speed Railways*, TB10621-2014, UDC, 2015.
[8] J. Kalibová, J. Petrů, and L. Jačka, "Impact of rainfall intensity on the hydrological performance of erosion control geotextiles," *Environmental Earth Sciences*, vol. 76, Article ID 429, 2017.
[9] J. Wang, Y. Xu, D. Zhang, and T. Gu, "Vibration-induced acceleration of infiltration in loess," *Science China Earth Sciences*, vol. 64, pp. 611–630, 2021.
[10] S. Zhao, J. Zheng, and J. Yang, "Stability analysis of embankment slope considering water absorption and sof-tening of subgrade expansive soil," *Water*, vol. 14, no. 21, Article ID 3528, 2022.
[11] A. Bridhikitti, P. Ruamchalerm, M. Keereesuwannakul, T. Prabamroong, G. Liu, and C. Huang, "Magnitude and factors influencing soil loss and sedimentation in the Mun river basin, Thailand," *CATENA*, vol. 210, Article ID 105872, 2022.
[12] A. A. Fenta, A. Tsunekawa, N. Haregeweyn et al., "Agroecology-based soil erosion assessment for better conservation planning in Ethiopian river basins," *Environmental Research*, vol. 195, Article ID 110786, 2021.
[13] L. Ben Cheikha, M. Jaoued, T. Aouadi, M. Ameur, and M. Gueddari, "Quantifying of water erosion and sediment yield by SEAGIS model in RMEL watershed (north–eastern Tunisia)," *Environmental Earth Sciences*, vol. 80, Article ID 790, 2021.
[14] C. Gobel and K. Lieberenz, *Handbook of Railway Geotechnical Buildings*, China Railway Publishing House Co., LTD, 2009.
[15] J. Fan, A. Motamedi, and M. Galoie, "Impact of *C* factor of USLE technique on the accuracy of soil erosion modeling in elevated mountainous area (case study: the Tibetan plateau)," *Environment, Development and Sustainability*, vol. 23, no. 8, pp. 12615–12630, 2021.
[16] Z. A. Gurmu, H. Ritzema, C. de Fraiture, M. Riksen, and M. Ayana, "Sediment influx and its drivers in farmers' managed irrigation schemes in Ethiopia," *Water*, vol. 13, no. 13, Article ID 1747, 2021.
[17] N. Nut, M. Mihara, J. Jeong et al., "Land use and land cover changes and its impact on soil erosion in stung sangkae catchment of Cambodia," *Sustainability*, vol. 13, no. 16, Article ID 9276, 2021.
[18] Y. Bai and H. Cui, "An improved vegetation cover and management factor for RUSLE model in prediction of soil erosion," *Environmental Science and Pollution Research*, vol. 28, pp. 21132–21144, 2021.
[19] A. Ghosh, S. Rakshit, S. Tikle et al., "Integration of GIS and remote sensing with RUSLE model for estimation of soil erosion," *Land*, vol. 12, no. 1, Article ID 116, 2023.
[20] B. Luo, H. T. Hu, and X. P. Lv, "Study on cutting slope surface erosion of granite eluvium in the south of China," *Journal of the Railway Engineering Society*, vol. 16, no. 3, pp. 82–85, 1999.
[21] Y. M. Wang, *Study on Erosion and Soil Stabilizer Properties for Highway Subgrade Slope (in Chinese)*, South China University of Technology, Guangzhou, Guangdong, 2003.
[22] Z. G. Li and X. Y. Zhang, "A energy-based erosion calculation model of the slopes for civil ergineering structures," *China Civil Engineering Journal*, vol. 38, no. 6, pp. 122–124, 2005.
[23] X. Kuang, *Research on the rules and evaluations of water erosion on railroad slopes*, PhD Thesis, Beijing Jiaotong University, 2009.
[24] Z. Guo, *Study on the Behavior and Laws Rainfall Erosion for Railway Embarkment Slope (in Chinese)*, China Academy of Railway Sciences, Beijing, 2012.
[25] L. Wang, R. Li, S. Zhang, R. Li, W. Bai, and H. Xiao, "Function of a deep-buried isolated trench and its effect on cracking failure characteristics of a slope under artificial rainfall," *Water*, vol. 14, no. 7, Article ID 1123, 2022.
[26] X. Y. Du, Z. Q. Guo, K. Chang, Z. L. Han, and J. T. Luo, "Research on slope topsoil instability mechanism of railway subgrade aiming at optimizing rainfall warning values," *Railway Engineering*, vol. 58, no. 1, pp. 47–50, 2018.
[27] G. R. Dou, "Incipient motion of sediment under currents," *China Ocean Engineering*, vol. 14, pp. 391–406, 2000.
[28] T. Ma, *Study on the Scour Mechanism of Wide-graded Earth-Rock Materials under the Condition of Overflowing Dam (in Chinese)*, Chongqing Jiaotong University, Chongqing, 2021.
[29] E. Shen, G. Liu, Y. Jia et al., "Effects of raindrop impact on the resistance characteristics of sheet flow," *Journal of Hydrology*, vol. 592, Article ID 125767, 2021.
[30] E. Shen, G. Liu, X. Xia et al., "Resistance to sheet flow induced by raindrop impact on rough surfaces," *CATENA*, vol. 231, Article ID 107272, 2023.